Journal of Materials Chemistry A

Accepted Manuscript

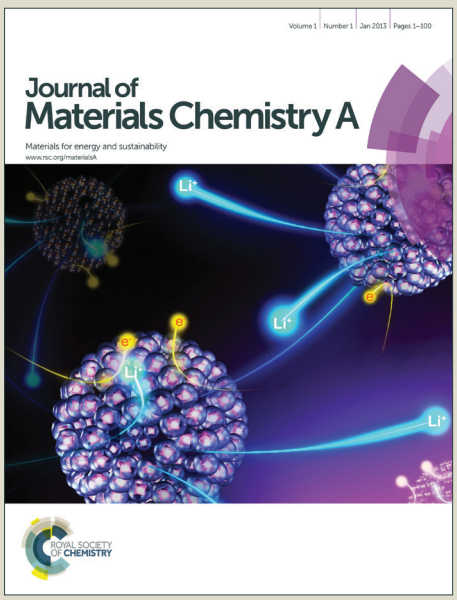

ROYAL SOCIETY OF CHEMISTRY

www.rsc.org/materialsA

Journal Name

RSCPublishing

ARTICLE

$CuInS_2$/ZnS nanocrystals as sensitisers for NiO photocathodes†

Cite this: DOI: 10.1039/x0xx00000x

Thomas J. Macdonald,[a] Yatin J. Mange, [a] Melissa R. Dewi, [a] Husn U. Islam,[bc] Ivan P. Parkin, [b] William M. Skinner [a] and Thomas Nann* [a]

Received 00th January 2012,
Accepted 00th January 2012

DOI: 10.1039/x0xx00000x

www.rsc.org/

Nickel oxide (NiO) is the most universally studied photocathode to date, however; their poor fill factors (*FFs*) make the efficiencies much lower than their counterpart, *n*-type photoanodes. Their significance in photovoltaics is based on the potential to fabricate tandem photoelectrodes in order to enhance the overall efficiency of existing devices. Furthermore, limited work on sensitising NiO with semiconducting nanocrystals (NCs) exists. For the first time, we have fabricated NiO photocathodes sensitised with aqueous $CuInS_2$/ZnS NCs. The NCs were chemically bound to NiO films with the aid of carboxyl and thiol groups. This was achieved without modifying the bulk surface properties of NiO. Binding of the NCs was investigated using TEM, SEM, XPS, XANES, EXAFS modelling and ToF-SIMS. NiO films were assembled into $CuInS_2$/ZnS NC sensitised photocathodes and their photovoltaic properties were compared to that of unsensitised and dye-sensitised NiO solar cells. We demonstrate that non-toxic NCs can be used to sensitise NiO photocathodes to achieve an (almost) all-inorganic system.

1 Introduction

Nickel oxide (NiO) is the most widely investigated photocathode to date where its use in *p*-type dye-sensitised solar cells (DSSCs) was first reported in 1999 by He *et al.* [1]. Since its discovery, there have been numerous publications highlighting the use of NiO as photocathodes for energy conversion [2–5]. The main interest in photocathodes is based on the potential to fabricate tandem solar cells as a cheap source of renewable energy, thus far the best performing tandem solar cell to date was reported by *Nattestad et al.* [4]. Recently, *Tain et al.* [6] achieved a remarkable 1.5 % efficiency for a perovskite-sensitised NiO photocathode. Despite this achievement, efficiencies of NiO photocathodes are typically less than 0.1%, which is still 100 times lower than most titanium dioxide (TiO_2) photoanodes [7]. NiO photocathodes are limited by their poor fill factor (*FF*) which are typically ~30% (less than half the *FF* for most TiO_2 DSSCs) [8,9]. Poor *FFs* of NiO DSSCs have been attributed to the existence of multiple pathways for charge recombination [9]. The limitations of poor *FFs* for *p*-type NiO solar cells have also been discussed by *Daeneke et al.* [10]. They explore the energy losses in NiO DSSCs and discovered that the poor FFs are partly due to recombination losses but could be minimised by the development of novel sensitisers and better electrolytes. In addition, poor sensitiser loading, high dark currents, low carrier mobility and small open circuit voltages (V_{OC}) all attribute to the low efficiencies of NiO photocathodes [2,3,5,7].

Early studies incorporated sensitising NiO photocathodes with an organic dye, coumarin (C343), a common *p*-type sensitiser [1,2,7,8,11]. While the C343-dye is certainly not the most efficient, it typically gives short circuit current density (J_{SC}) values between 0.5 and 1 mA/cm^2 and is still the most studied *p*-type sensitiser to date [12]. The most efficient dyes are the π-conjugated perylenemonoimide (PMI) electron acceptors [4,12]. While other PMI-based donor-acceptor type dyes have been studied [4,11]. Until now, there are limited publications which describe sensitising NiO photocathodes with semiconducting nanocrystals (NCs) [13,14]. Recent work by *Barcelo et al.* and *Park et al.* [13,14] report sensitising NiO with NCs, however both studies incorporate the use of cadmium selenide (CdSe) NCs. Incorporating chalcogenides which contain heavy metals is not a favourable approach due to toxicity. In contrast, this study reports on sensitising NiO photocathodes with copper indium disulfide ($CuInS_2$/ZnS) NCs. $CuInS_2$/ZnS NCs are non-toxic and inexpensive alternatives to toxic NCs and costly dye molecules. NiO has been shown to be efficient at transporting and collecting holes in NC loaded devices [15,16]. The charge transfer process in a NC sensitised photocathode requires 3 steps. Firstly, photo-excitation of the exciton, followed by the injection of holes from the VB of the NC to the NiO, and finally an electron transfer. While this process has been studied before, we study the surface chemistry of $CuInS_2$/ZnS NC covalently bound to NiO for their use as NC sensitised photocathodes.

$CuInS_2$ NCs were first reported by *Castro et al.* [17]. Since their discovery in 2003, there has been vast improvements in both their stability [18] and use in application [19,20]. While our earlier work focused on the synthesis and optical tuning of aqueous $CuInS_2$/ZnS NCs, this work investigates the surface chemistry and immobilisation on NiO photocathodes. Direct deposition (drop casting) with the aid of bifunctional linker molecules is a common approach to get NCs on a surface, [14,21–24] particularly for NCs dispersed in organic solvents. Electrophoretic deposition (EDP), is another popular deposition technique where recent work by *Jara et al.* established an *n*-type $CuInS_2$ solar cell using EPD and achieved an efficiency of 2.52% [25]. A more attractive approach for NC attachment can be achieved by incorporating the use of polar solvents. While successive ionic layer adsorption and reaction (SILAR) is a popular method for nanoparticle attachment [26,27], our approach incorporates binding $CuInS_2$/ZnS NCs with the assistance of mercaptoacetic acid (MAA). MAA contains both carboxyl and thiol groups to stabilise the NCs on the surface of NiO photocathodes. While the approach was initially reported by *Hu et al.* [28] with TiO_2, this is the first time the method has been combined with a *p*-type photocathode like NiO. While $CuInS_2$ NCs clearly exhibit many exciting properties, it is their non-toxic credibility that makes them attractive alternatives to the commonly used cadmium and lead containing NCs. While $CuInS_2$ NCs have been previously used as sensitisers for TiO_2 photoanodes, [18–20,29–31] this is the first example of a NiO photocathode sensitised with heavy metal free NCs. It is also the first method of chemical attachment from an aqueous dispersion of NCs bound to NiO.

2. Experimental Section

2.1 Synthesis of aqueous $CuInS_2$/ZnS NCs

$CuInS_2$/ZnS NCs were synthesised according to our previous report [31]. Briefly, 0.5 mL $Cu(Ac)_2$ (0.125 M) and 0.5 mL $InCl_3$ (0.125 M) were injected into 37.5 mL of Milli-Q water at ambient temperature. 0.25 mL of mercaptoacetic acid (1:5) aqueous solution was then injected to the mixture. Upon injection, the clear solution changed to black before changing back to clear. Adding ~1 mL of NaOH then neutralised the pH of the solution. Once the solution was neutralised (pH 7), 0.25 mL of Na_2S (0.5 M) was injected causing an immediate deep red colour change. The NC solution was then transferred to a Teflon-lined dialysis chamber to remove the unreacted products such as excess mercaptoacetic acid. Cation exchange was performed by adding 10 mM of $Zn(Ac)_2$ and allowing the solution to stir at ambient temperature over night. $CuInS_2$/ZnS NCs were precipitated using methanol.

2.2 NiO paste and film preparation

5 µM thick NiO photocathodes were prepared by creating a slurry of NiO nanoparticles (Sigma). Firstly, 0.5 g of NiO nanopowder was added to 20 mL of ethanol and sonicated for 4 hours. ~ 3 mL of terpineol was then added and the slurry was further sonicated for a further 2-3 hours or until NiO agglomerates were gone. Finally, ethanol was removed by slow rotary evaporation. NiO paste was applied to pre-cleaned 15-Ω/cm^2 fluorine-doped tin oxide (Solaronix) by doctor blade technique. Finally, NiO photocathodes were sintered in an oxygen furnace for 2 hours at 500 °C.

2.3 Film sensitising

NiO photocathodes were stored at 100 °C prior to sensitising with $CuInS_2$/ZnS NCs. NiO photocathodes were soaked in a concentrated solution of $CuInS_2$/ZnS NCs under dark conditions for 48 hours. Covalent attachment of the NCs was achieved with the assistance of MAA through carboxyl and thiol bond stabilisation on the NiO surface. NC sensitised NiO photocathodes were washed with milliQ water and tested immediately in a *p*-type sandwich style solar cell configuration.

2.4 Fabrication of solar cell

Counter electrodes of platinum coated fluorine tin oxide (FTO) were used in the solar cells (Dyesol). Surlyn™ (Solaronix) was used as a thermoplastic gasket and placed between the platinum counter electrode and NC sensitised NiO photocathode. The assembled device was then clamped and maintained at 100 °C for 15 minutes to set the gasket, sealing the device. The regular geometry of the device was 1 cm x 0.45 cm with an active cell area of 0.45 cm^2. The iodide/triodide (I^-/I_3^-) redox mediator was prepared according to a previous report [32]. Briefly, the redox mediator consisted of 1-propyl 3-methylimidazolium iodide (0.8 M), iodine (0.1 M) and benzimidazole (0.3M) in 3-methoxypropionitrile (Sigma Aldrich).

2.5 Characterisation

Photoluminescence spectroscopy and Quantum Yield measurements were carried out on an Edinburgh Instruments Fluorometer FLS980. UV-Visible spectroscopy measurements were carried out on an Agilent Cary 300 spectrometer. Transmission Electron Microscopy was carried out on a JEOL JEM-2100F with an acceleration voltage of 200 kV. Scanning electron microscopy images were obtained on a FEI Quanta 450 Environmental Scanning Electron Microscope (ESEM, University of Adelaide). X-ray photoelectron spectroscopy (XPS) measurements were recorded on a Thermo Scientific K-alpha spectrometer at University College London. Time-of-Flight Secondary Ion Mass Spectrometry (ToF-SIMS) was used to perform elemental depth profiles on $CuInS_2$/ZnS sensitised NiO photocathodes. The ToF-SIMS instrument was a Physical Electronics TRIFT V NanoToF. Depth profiles were conducted using a single Au 30keV LMIG source operating in pulsed and continuous modes for analysis and sputtering cycles respectively. Film thicknesses were measured using a Profilometer (Bruker, Dektak XT) with Vision64 software and a stylus force set to 0.3 mg to scan across the groove. *JV*-curves were acquired with a Keithley 2601 source measure unit and recorded using a custom LabVIEW™ virtual instrument. The solar cells were illuminated with 100 mW/cm^2 light from Xenon-arc source passed through an AM1.5G filter (Abet Technologies Solar Simulator) at 25 °C. The illumination plane for the light source was calibrated with a monocrystalline silicon reference cell (91150V, Newport). Diffuse reflectance UV-Visible spectroscopy was measured using a Perkin-Elmer Lambda 950 UV-Vis NIR with 150 mm integrating sphere at Flinders University.

2.6 ESRF

XANES and EXAFS measurements were performed on the Dutch-Belgian EXAFS beamline, BM26A, at the ESRF. Data was acquired in fluorescence mode using an ionisation chamber for incident beam detection, and a 9 element germanium solid state fluorescence detector. Monochromated beam was achieved with a Si(111) double crystal monochromator. Data for the NiO film was acquired on the Ni K-edge (ca. 8333 eV), and data for the QD sensitised NiO film was acquired on the Ni K-edge, and Zn K-edge (ca. 9664 eV). Data reduction and EXAFS modelling were performed on Horae Athena and Excurve 9.273 respectively [33,34].

3 Results

3.1 Spectroscopy NCs

Figure 1a shows the absorbance and emission spectrum for $CuInS_2$/ZnS NCs. While the absorbance spectrum shows a broad peak, no strong excitonic peak is present. The broad features for the absorption spectrum and lack of excitonic peak has been reported previously and attributed to surface defects in the NCs [25,31]. The absorbance and emission spectrum of $CuInS_2$ core NCs, may be found in the supporting information (ESI), **Figure S1**. The broad emission peak for the $CuInS_2$/ZnS NCs appears in the visible region at 590 nm, the tail end of the peak stretches out across the infrared region, consistent with the emission spectra for $CuInS_2$/ZnS NCs [31,35]. The full width at half maximum (FWHM) was measured to be 109 nm, slightly narrower than our last reported FWHM for $CuInS_2$/ZnS NCs [31]. Our previous study discusses the presence of two shoulders in the emission spectra for $CuInS_2$ core shell NCs, one at 535 nm and the other at 690 nm. While we may argue a slight shoulder is present at 700 nm for the $CuInS_2$/ZnS NCs in **Figure 1a**, we no longer see a shoulder at lower emission. As originally hypothesised by our previous study, these shoulders are not present, suggesting copper vacancies are in-fact being filled by zinc [31]. A Gaussian function of the emission spectra was also fitted to indicate a bimodal distribution for the emission spectra. In order to help elude the physical properties for the NCs, the band gap for was calculated to be ~2.04 eV from the absorption tauc plot in **Figure 1b**. This calculation was further verified by the reflectance spectrum (inset **Figure 1b**). The previous study revealed that as the concentration of zinc increases, the defect at lower emission disappears. In this manuscript, we manage to increase the concentration of ZnS to 10 mM without salting out the colloid. While this is a significant increase in concentration from our previous work, it was found to be the optimum state for stability with the NCs lasting several weeks in an oxygen atmosphere. The quantum yield of these NCs was measured to be 1.5 %. Since defects have been reduced, the higher quantum yield may be due to better lattice matching between the core NCs and ZnS. Lattice matching is vital in both reducing surface defects and increasing the quantum yield [36].

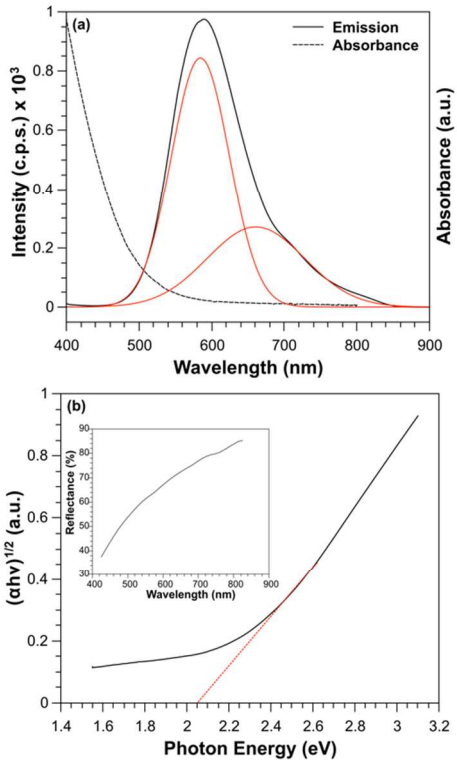

Figure 1. (a) Emission and absorbance spectrum for aqueous $CuInS_2$/ZnS quantum dots. The red line indicates the Gaussian fit for emission curve. (b) Tauc abosprtion plot for band gap estimation. Inset represents the reflectance spectrum for $CuInS_2$/ZnS further verifying band gap estimation.

3.2 TEM and SEM

$CuInS_2$/ZnS NCs were synthesised by methods described previously [31]. **Figure 2a** shows transmission electron microscopy (TEM) of the NCs. The average particle size was found to be 12.22 ± 0.052 nm, consistent with $CuInS_2$/ZnS NCs [30,35]. Additional TEM images including particle size distribution (histogram) and dynamic light scattering measurements (DLS) may be found in **Figure S2,** ESI. The lattice spacing was 0.32 nm (**Figure 2b**), consistent with $CuInS_2$/ZnS NCs [37]. The lattice spacing was in agreement with the 112 plane from the X-ray diffraction (XRD) measured from our previous work [31]. Additional XRD for these synthesised NCs along with the selected area diffraction (SAED) may be found in **Figure S3**, ESI. The attachment of $CuInS_2$/ZnS NCs to NiO was also investigated using TEM. **Figure 2c** shows NiO photocathodes before sensitising with NCs. **Figure 2d** shows NiO photocathodes after sensitising with NCs, the images of the sensitised NiO are consistent with TEM in the literature [13]. The NCs are scattered throughout the film and are indicated by the red circles. For further verification, energy dispersed X-Ray spectroscopy (EDXS) was measured on both the unsensitised and NC sensitised NiO photocathodes. The EDXS shows the presence of copper, indium, sulphur and zinc ions only on the sensitised NiO photocathodes (EDXS shown in **Figure S4,** ESI).

Scanning electron microscopy (SEM) is shown in **Figure S5**, ESI**.** SEM shows a rigid structure of NiO photocathodes. The films appear to have some cracks which are due to possible NiO particle agglomerates and thickness of the film. While previous studies incorporate thinner films, we choose to increase the thickness of the NiO because it has been found that improved NC loading can be achieved with thicker films [13]. Thicker NiO films with substantially higher NC loading has been found to also dramatically improve the photocurrent response [13].

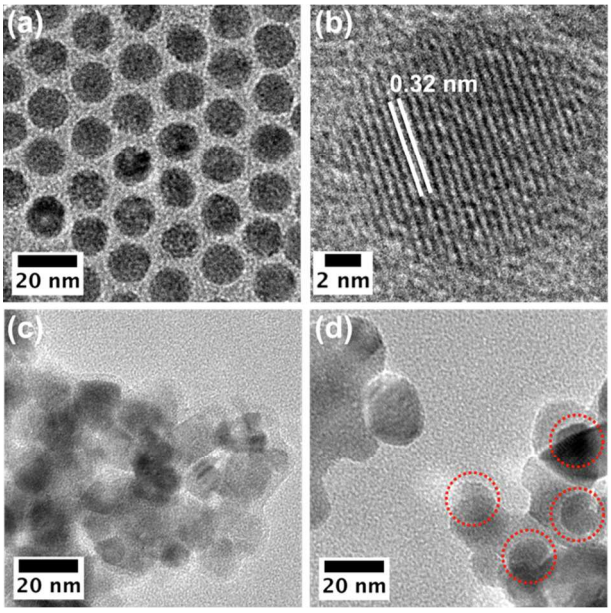

Figure 2. High resolution TEM for $CuInS_2$/ZnS NCs and NiO photocathodes. (a) $CuInS_2$/ZnS NCs HRTEM. (b) Lattice fringes of $CuInS_2$/ZnS NCs shown tob e 0.32 nm. (c) NiO photocathode film without NCs. (d) NiO photocathode film with NCs.

3.3 XPS and ToF-SIMS

The chemical composition of the $CuInS_2$/ZnS NCs on NiO photocathodes was measured using XPS (Figure 3). Binding energies were charge corrected against C 1 before the high resolution XPS was annotated. The survey spectra for NCs on NiO photocathodes represents labeled core states (Ni 2p, Cu 2p, In 3d, S 2p, and Zn 2p) and is supplied in Figure S6a, ESI. Also in the ESI is the high resolution Ni 2p for unsensitised NiO photocathodes (Figure S6b, ESI). Figure 3a represents the Ni 2p spectra showing core splitting into Ni $2p_{3/2}$ (854.2 eV) and Ni $2p_{1/2}$ (872.5 eV) with a peak separation of 18.3 eV. In addition, corresponding satellite peaks are present at 861.2 eV and 879.5 eV, respectively. The results are consistent with Ni(II) in NiO [38–40]. There was no change in the XPS spectra for the unsensitised NiO photocathodes (Figure S6b), suggesting the immobilisation of $CuInS_2$/ZnS does not cause any differences in the chemical composition of NiO.

Figure 3b shows narrow Cu 2p doublets at Cu $2p_{3/2}$ (932.7 eV) and Cu $2p_{1/2}$ (952.6 eV) with a peak separation of 19.9 eV. The results are consistent with Cu(I) species in a sulphide environment, in agreement with previous reports [41–43]. Furthermore, the Cu 2p spectra showed no evidence of Cu(II) species on the surface of the $CuInS_2$/ZnS NCs. This has been recognised previously and attributed to the absence of the Cu(II) 'shake up' satellites [44–46].
In 3d peaks are shown in Figure 3c which show spin-orbit splitting of 7.6 eV with the In $3d_{5/2}$ and In $3d_{1/2}$ at 445.1 eV and 452.7 eV, respectively. This is indicative of In(III) with reference to previous reports [41–43].

The S 2p is shown in Figure 3d and consists of an envelope centred near 162.7 eV comprising more than one characteristic S 2p doublet. Fitting of the envelope required two S 2p doublets, comprising S $2p_{3/2}$ and S $2p_{1/2}$ components separated by ~1.2 eV spin-orbit splitting and in the branching ratio of 2:1 [47]. The fit result is shown in Figure 3d and suggests two sulphur environments. These are located at an S $2p_{3/2}$ situated at binding energies of 161.9 eV and 162.9 eV respectively. The component at 162.9 eV binding energy is entirely consistent with sulphur in CIS environment, i.e. co-ordinated with two Cu and two In atoms in the lattice, [44,48] similar to the natural mineral chalcopyrite, $CuFeS_2$ [49]. The component at 161.9 eV binding energy is assigned to sulphur in a ZnS environment, [50,51] consistent with sphalerite or wurtzite, and reported previously [31]. Zn 2p is shown in Figure 3e and is split into Zn 2p3/2 (1021.2 eV) and Zn 2p1/2 (1044.3 eV), this can be assigned to Zn(II) with a peak separation of 22.9 eV [42,52].

Time of flight secondary ion mass spectroscopy (ToF-SIMS) further verified the covalent attachment of $CuInS_2$/ZnS NCs on the surface of NiO photocathode films. The ToF-SIMS depth profile shown in Figure S7, ESI indicated that our NCs are rich in Cu and Zn ions near the surface which is consistent with our previous report [31]. While this was expected for the Cu ions, the strong presence of Zn is thought to be due to oxidation near the surface.

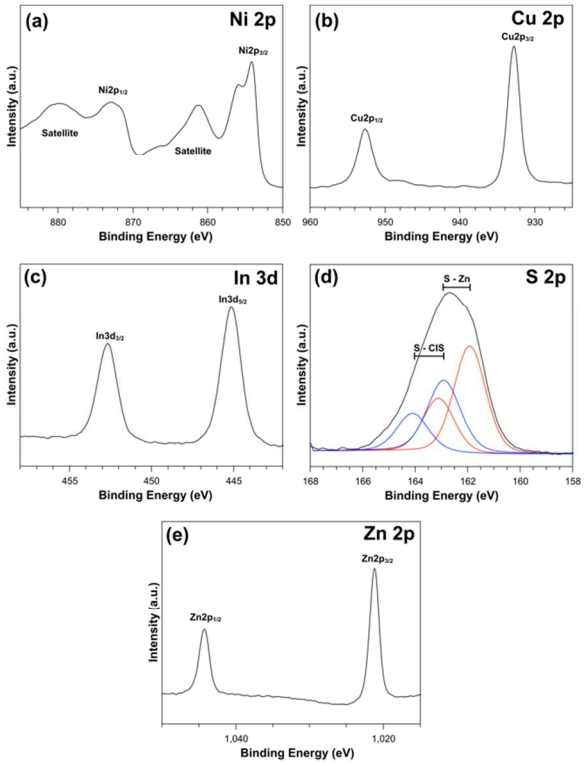

Figure 3. High resolution XPS for $CuInS_2$/ZnS on NiO photocathodes. The specra represents Ni 2p (a), Cu 2p (b), In 3d (c), S 2p (d) and Z 2p (e).

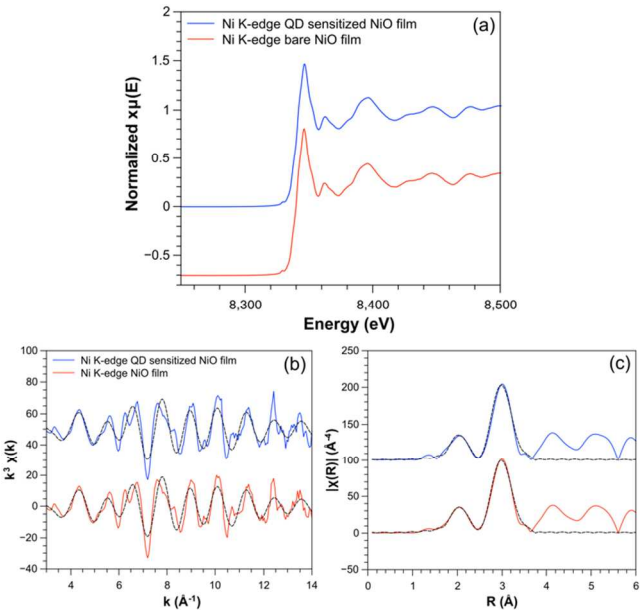

Figure 4. Nickel K-edge (a) XANES, (b) EXAFS and (c) Fourier transform of NC sensitised NiO (blue) and unsensitised NiO (red). The solid lines represent experimental data and dashed lines denotes the theoretical model.

3.4 XANES and EXAFS

Ni K-edge XANES and EXAFS analysis confirm an absence of local structural change in the NiO film upon sensitisation with NCs. The similar XANES of the NC sensitised and unsensitised NiO photocathode films are shown in **Figure 4a.** EXAFS analysis shows that the local structures of both are in good agreement with the known NiO XRD structure (**Figure 4b** and **Figure 4c, Table 1**).[53] From the EXAFS, the bond distance of Ni-O was found to be 2.08±0.01 Å, which compared to the XRD of 2.089 Å for both unsenstised and NC sensitised NiO photocathodes (**Table 1**). This may suggest that the NCs are not chemically integrated into the NiO system or there is very little coating to affect the bulk of the NiO.

Table 1. EXAFS Nickel K-edge for unsensitised and NC sensitised NC photocathodes

Film	Scatter	*N*	R_{XRD} (Å)	R_{EXAFS} (Å)	$2\sigma^2$ (Å^2)	*F*
NiO	O	6	2.089	2.08±0.01	0.012	57
	Ni	12	2.954	2.95±0.01	0.012	
NiO NCs	O	6	2.089	2.08±0.01	0.012	59
	Ni	12	2.954	2.95±0.01	0.011	

Figure 5a shows the Zn K-edge XANES for the NC sensitised NiO photocathode films. The XANES spectroscopy is consistent with Zn K-edge reported previously for ZnO [54]. First shell EXAFS analysis of the NC sensitised NiO at the zinc K-edge reveals the coexistence of two local environments consisting of zinc-oxygen and zinc-sulphur bonds (**Figure 5b** and **Figure 5c**). Refinement of the coordination number and bond distances of the Zn-O and Zn-S paths reveal 68 ± 8 % Zn-O bond distances at 2.04Å and 33 ± 5 % Zn-S bond distances at 2.31Å indicating significant oxide formation around the zinc constituent in the material (**Table 2**). The bond distances for Zn-O and Zn-S were both consistent with literature.

Cu K-edge data was not obtained due to high levels of noise from Ni fluorescence.

Table 2. EXAFS Zn K-edge for NiO + NCs Film

Sample	Scatter	Ratio %	*N*	R_{EXAFS} (Å)	$2\sigma^2$ (Å^2)	*F*
Zn K-edge	O	68 ± 8	4	2.04± 0.04	0.008	54
Zn K-edge	S	33 ± 5	4	2.31± 0.05	0.013	54

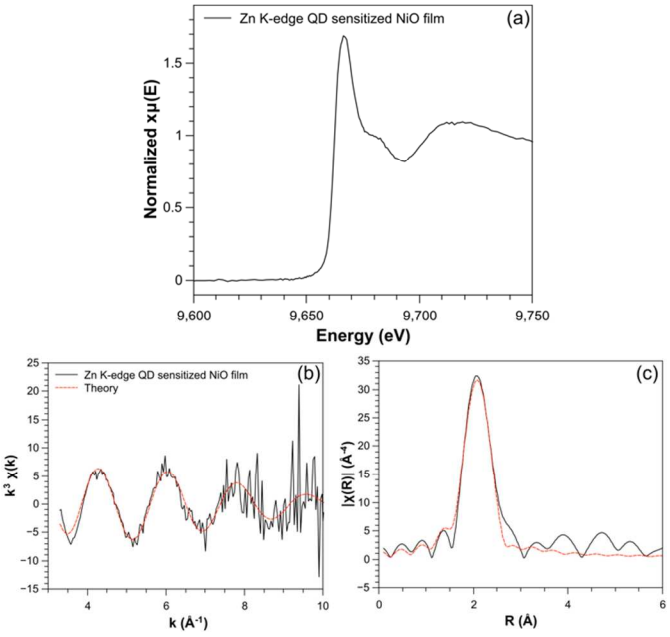

Figure 5. Zinc K-edge (a) XANES, (b) EXAFS and (c) Fourier transform of NC sensitised NiO (black). The solid lines (black) represent experimental data and dashed lines (red) denotes the theoretical model.

3.5 Photovoltaic measurements

Notwithstanding the recent success with *p*-type NiO DSSCs, the successful binding of $CuInS_2$/ZnS NCs onto NiO allowed us to test this new photocathode as a *p*-type photovoltaic device. Knowing that the C343-dye is commercially available and the most studied dye-sensitiser, prompted us to use it as a standard comparison for the *p*-type PV devices. Initially we tested the device with a polysulfide electrolyte to avoid photocorrosion of the NCs. While this failed to provide any substantial photocurrents, we tested our system with the common DSSC redox mediator ioidide/triiodide (I^-/I_3^-). Although we were initially concerned with photocorrosion of the NCs, the I^-/I_3^- redox mediator provided more promising results than the polysulfide redox couple. Even though using corrosive redox mediators for NCs sensitised solar cells is not a common approach, in order to compare our results to that of the C343-dye, the I^-/I_3^- redox mediator was required.

Figure 6 shows light *JV*-curves for NiO, NiO + $CuInS_2$/ZnS and NiO + C343-Dye. The *JV*-curves show that the $CuInS_2$/ZnS NCs (***η*:** 0.01%) are three times lower in efficiency than the C343-dye (***η*:** 0.03%**).** While the NC sensitised NiO photocathodes measured J_{SC}: 0.56 mA/cm^2 (0.16 μA/cm^2 higher than the unsensitised sample), the poor V_{OC}**:** 0.055 V and **FF:** 25%, affected the overall performance of this device. The J_{SC}, V_{OC} and ***FF*** values for the C343-dye-sensitised NiO photocathodes are comparable to those reported in literature [12]. A detailed description of the redox reaction between our photocathode systems can be found in **S8**, ESI. Dark currents for NC and C343-Dye-senstised NiO photocathodes can be seen in **Figure S9**,ESI. High dark currents have been previously attributed to recombination of holes in the NiO with the donar species (I_3^-) [55]. The inset for Figure 6 shows the diffuse reflectance absorption spectra for each of the NiO photocathodes. For the NiO photocathodes sensitised with $CuInS_2$/ZnS NCs, the light absorption extends to the visible region, which corresponds to the absorption spectra of the NCs discussed earlier in the manuscript. The absorption of the C343-dye corresponds in a similar way.

Further studies incorporating more suitable electrolytes may help improve the efficiency of this device. Studies on a wider range of wavelengths (quantum efficiency) and charge separation need to be considered. **Table 3** shows a summary of the photovoltaic performance for NiO photocathodes (unsenstised), sensitised with NCs and C343-Dye. Despite the novel approach of covalently binding the NCs to NiO photocathodes, the photovoltaic performance from C343-Dye outperformed the NCs. This may be due to insufficient NC loading or interference from the organic ligands between the terminals, slightly insulating the solar cell. Poor NC loading may be improved by measuring molar absorptions and the insulating ligands may be removed by investigating different sintering temperatures. In addition, stability measurements were carried out after a 6-hour time period ruling out possible photocorrosion (**S10** table S1, ESI).

Table 3. Photovoltaic performance of NiO photocathodes of iodideconcentrations < 0.1M (**S11**, ESI)

Sample	V_{OC} (mV)	J_{SC} (mA/cm^2)	*FF* %	*η* %	Ref.
NiO	88	0.40	29	0.01	N/A
NiO + NCs	56	0.57	26	0.01	N/A
NiO + C343	100	0.98	30	0.03	N/A
NiO + C343	98	0.55	29	0.02	[8]
NiO + C343	101	0.86	36	0.03	2]2
NiO + C343	105	0.21	33	0.01	5556

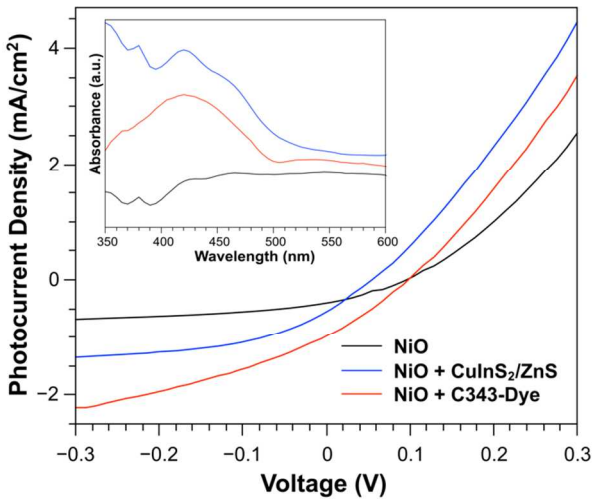

Figure 6. Light *JV*-Curves for NiO Photocathodes (unsensitised), sensitised with $CuInS_2$/ZnS NCs and C343-dye. The illuminated cell area was 0.45 cm^2. The inset shows the diffuse reflectance absorbance spectra for the corresponding photocathode films.

4. Conclusions

We have successfully attached aqueous $CuInS_2$/ZnS NCs to *p*-type NiO photocathodes. Extensive surface characterisation has proven the covalent attachment of the NCs. It was found that despite modifying the surface of NiO with NCs, it has no effect on the surface properties of bulk NiO. This was investigated using TEM, XPS, XANES, EXAFS modelling and ToF-SIMS. While the surface properties from sensitising were not altered, the optical properties were affected by the sensitising of NCs. Assembling the NiO films into sensitised photocathodes and measuring their photovoltaic properties investigated this. It was found that the NC sensitised NiO photocathodes were responsive to AM 1.5 visible light and had a J_{SC} of 0.58 mA/cm^2. Despite the novelty of sensitising NiO with non-toxic NCs, poor V_{OC} and *FF* values limit the overall efficiency of the device. Future work includes incident photon conversion efficiencies as well as a more detailed study into the depth of the charge transfer mechanics between NiO and $CuInS_2$/ZnS NCs.

Acknowledgements

This work was performed in part at the South Australian node of the Australian National Fabrication Facility (ANFF), a company established under the National Collaborative Research Infrastructure Strategy to provide nano and micro-fabrication facilities for Australia's researchers. Dr. Robert R. Palgrave at the Department of Chemistry, University College London, undertook the X-ray photoelectron spectroscopy measurements. We would like to acknowledge the Graduate Research Centre of the University of South Australia for partially funding the work completed at University College London. We acknowledge the European Synchrotron Radiation Facility for provision of synchrotron radiation facilities and we would like to thank Dr Dipanjan Banerjee for assistance in using the Dutch-Belgian EXAFS beamline, BM26A. The authors would finally like to acknowledge Dr. Daniel D. Tune and Prof. Joseph G. Shapter for their assistance with the photovoltaic set up.

Notes

[a] Ian Wark Research Institute, University of South Australia,
Mawson Lakes Blvd, Adelaide, SA 5095, Australia.
E-Mail: thomas.nann@unisa.edu.au
[b] Department of Chemistry, University College London,
20 Gordon St, London, WC1H 0AJ, United Kingdom
[c]ESRF, The European Synchrotron, 71 Avenue des Martyrs
38000 Grenoble, France

†. Electronic Supplementary Information (ESI) available: [details of any supplementary information available should be included here]. See DOI: 10.1039/b000000x/

References

1 J. He, H. Lindström, A. Hagfeldt and S.-E. Lindquist, *J. Phys. Chem. B*, 1999, **103**, 8940–8943.
2 S. Mori, S. Fukuda, S. Sumikura, Y. Takeda, Y. Tamaki, E. Suzuki and T. Abe, *J. Phys. Chem. C*, 2008, **112**, 16134–16139.
3 E. A. Gibson, A. L. Smeigh, L. Le Pleux, J. Fortage, G. Boschloo, E. Blart, Y. Pellegrin, F. Odobel, A. Hagfeldt and L. Hammarström, *Angew. Chem. Int. Ed.*, 2009, **48**, 4402–4405.
4 A. Nattestad, A. J. Mozer, M. K. R. Fischer, Y.-B. Cheng, A. Mishra, P. Bauerle and U. Bach, *Nat Mater*, 2010, **9**, 31–35.
5 Z. Ji, G. Natu, Z. Huang and Y. Wu, *Energy Environ. Sci.*, 2011, **4**, 2818–2821.
6 H. Tian, B. Xu, H. Chen, E. M. J. Johansson and G. Boschloo, *ChemSusChem*, 2014, **7**, 2150–2153.
7 Y. Qu, W. Zhou, X. Miao, Y. Li, L. Jiang, K. Pan, G. Tian, Z. Ren, G. Wang and H. Fu, *Chem. – Asian J.*, 2013, n/a–n/a.
8 A. Nattestad, M. Ferguson, R. Kerr, Y.-B. Cheng and U. Bach, *Nanotechnology*, 2008, **19**.
9 L. D'Amario, L. J. Antila, B. Pettersson Rimgard, G. Boschloo and L. Hammarström, *J. Phys. Chem. Lett.*, 2015, 779–783.
10 T. Daeneke, Z. Yu, G. P. Lee, D. Fu, N. W. Duffy, S. Makuta, Y. Tachibana, L. Spiccia, A. Mishra, P. Bäuerle and U. Bach, *Adv. Energy Mater.*, 2014, n/a–n/a.
11 A. Morandeira, J. Fortage, T. Edvinsson, L. Le Pleux, E. Blart, G. Boschloo, A. Hagfeldt, L. Hammarstrom and F. Odobel, *J. Phys. Chem. C*, 2008, **112**, 1721–1728.
12 F. Odobel, L. Le Pleux, Y. Pellegrin and E. Blart, *Acc. Chem. Res.*, 2010, **43**, 1063–1071.
13 I. Barceló, E. Guillén, T. Lana-Villarreal and R. Gómez, *J. Phys. Chem. C*, 2013, **117**, 22509–22517.
14 M.-A. Park, S.-Y. Lee, J.-H. Kim, S.-H. Kang, H. Kim, C.-J. Choi and K.-S. Ahn, *Phys. Status Solidi A*, 2014, **211**, 1868–1872.
15 X. Wu and E. K. L. Yeow, *Chem. Commun.*, 2010, **46**, 4390–4392.
16 J.-M. Caruge, J. E. Halpert, V. Bulović and M. G. Bawendi, *Nano Lett.*, 2006, **6**, 2991–2994.
17 S. L. Castro, S. G. Bailey, R. P. Raffaelle, K. K. Banger and A. F. Hepp, *Chem. Mater.*, 2003, **15**, 3142–3147.
18 T.-L. Li and H. Teng, *J Mater Chem*, 2010, **20**, 3656–3664.

19 X. Hu, Q. Zhang, X. Huang, D. Li, Y. Luo and Q. Meng, *J Mater Chem*, 2011.
20 J. Luo, H. Wei, Q. Huang, X. Hu, H. Zhao, R. Yu, D. Li, Y. Luo and Q. Meng, *Chem. Commun.*, 2013, **49**, 3881–3883.
21 S. Chandrasekaran, T. J. Macdonald, Y. J. Mange, N. H. Voelcker and T. Nann, *J. Mater. Chem. A*, 2014, **2**, 9478–9481.
22 T. Nann, S. K. Ibrahim, P.-M. Woi, S. Xu, J. Ziegler and C. J. Pickett, *Angew. Chem. Int. Ed.*, 2010, **49**, 1574–1577.
23 T. J. Macdonald and T. Nann, *Nanomaterials*, 2011, **1**, 79–88.
24 D. P. Tran, T. J. Macdonald, B. Wolfrum, R. Stockmann, T. Nann, A. Offenhäusser and B. Thierry, *Appl. Phys. Lett.*, 2014, **105**.
25 D. H. Jara, S. J. Yoon, K. G. Stamplecoskie and P. V. Kamat, *Chem. Mater.*, 2014, **26**, 7221–7228.
26 H. Lee, M. Wang, P. Chen, D. R. Gamelin, S. M. Zakeeruddin, M. Grätzel and M. K. Nazeeruddin, *Nano Lett.*, 2009, **9**, 4221–4227.
27 Z. Zhou, S. Yuan, J. Fan, Z. Hou, W. Zhou, Z. Du and S. Wu, *Nanoscale Res. Lett.*, 2012, **7**, 1–8.
28 X. Hu, Q. Zhang, X. Huang, D. Li, Y. Luo and Q. Meng, *J Mater Chem*, 2011.
29 T.-L. Li, Y.-L. Lee and H. Teng, *J. Mater. Chem.*, 2011, **21**, 5089–5098.
30 S. Peng, F. Cheng, J. Liang, Z. Tao and J. Chen, *J. Alloys Compd.*, 2009, **481**, 786–791.
31 T. J. Macdonald, Y. J. Mange, M. Dewi, A. McFadden, W. M. Skinner and T. Nann, *CrystEngComm*, 2014.
32 D. D. Tune, B. S. Flavel, J. S. Quinton, A. V. Ellis and J. G. Shapter, *Sol. Energy Mater. Sol. Cells*, 2010, **94**, 1665–1672.
33 B. Ravel and M. Newville, *J Synchrotron Rad*, 2005, **12**.
34 N. Binsted, *Excurv98 CCLRC Daresbury Lab. Comput. Program*, 1998.
35 J. Park and S.-W. Kim, *J Mater Chem*, 2011, **21**, 3745–3750.
36 J. C. Bear, N. Hollingsworth, A. Roffey, P. D. McNaughter, A. G. Mayes, T. J. Macdonald, T. Nann, W. H. Ng, A. J. Kenyon, G. Hogarth and I. P. Parkin, *Adv. Opt. Mater.*, 2015, n/a–n/a.
37 B. Cichy, D. Wawrzynczyk, A. Bednarkiewicz, M. Samoc and W. Strek, *RSC Adv.*, 2014, **4**, 34065–34072.
38 T. J. Macdonald, J. Xu, S. Elmas, Y. J. Mange, W. M. Skinner, H. Xu and T. Nann, *Nanomaterials*, 2014, **4**, 256–266.
39 A. P. Grosvenor, M. C. Biesinger, R. S. C. Smart and N. S. McIntyre, *Surf. Sci.*, 2006, **600**, 1771–1779.
40 Z. Yin, N. Chen, F. Yang, S. Song, C. Chai, J. Zhong, H. Qian and K. Ibrahim, *Solid State Commun.*, 2005, **135**, 430–433.
41 Q. Li, C. Zou, L. Zhai, L. Zhang, Y. Yang, X. Chen and S. Huang, *CrystEngComm*, 2013, **15**, 1806–1813.
42 H. Shen, H. Yuan, F. Wu, X. Bai, C. Zhou, H. Wang, T. Lu, Z. Qin, L. Ma and L. S. Li, *J. Mater. Chem.*, 2012, **22**, 18623–18630.
43 H. Zhong, Y. Zhou, M. Ye, Y. He, J. Ye, C. He, C. Yang and Y. Li, *Chem. Mater.*, 2008, **20**, 6434–6443.
44 T. J. Macdonald, Y. J. Mange, M. Dewi, A. McFadden, W. M. Skinner and T. Nann, Engineers Australia, 2013.
45 W. M. Skinner, C. A. Prestidge and R. S. C. Smart, *Surf. Interface Anal.*, 1996, **24**, 620–626.
46 A. N. Buckley, W. M. Skinner, S. L. Harmer, A. Pring, R. N. Lamb, L.-J. Fan and Y. Yang, *Can. J. Chem.*, 2007, **85**, 767–781.
47 G. U. Von Oertzen, W. M. Skinner and H. W. Nesbitt, *Phys. Rev. B*, 2005, **72**.
48 C. C. Landry and A. R. Barron, *Science*, 1993, **260**, 1653–1655.
49 S. R. Grano, M. Sollaart, W. Skinner, C. A. Prestidge and J. Ralston, *Int. J. Miner. Process.*, 1997, **50**, 1–26.
50 T. N. Khmeleva, W. Skinner and D. A. Beattie, *Int. J. Miner. Process.*, 2005, **76**, 43–53.
51 C. A. Prestidge, W. M. Skinner, J. Ralston and R. S. . Smart, *Appl. Surf. Sci.*, 1997, **108**, 333–344.
52 A. Singh, H. Geaney, F. Laffir and K. M. Ryan, *J. Am. Chem. Soc.*, 2012, **134**, 2910–2913.
53 T. Y. Sasaki Satoshi, *Proc Jpn. Acad. Ser. B*, 1979, **55**, 43–48.
54 I. Perelshtein, E. Ruderman, N. Perkas, T. Tzanov, J. Beddow, E. Joyce, T. J. Mason, M. Blanes, K. Molla, A. Patlolla, A. I. Frenkel and A. Gedanken, *J. Mater. Chem. B*, 2013, **1**, 1968–1976.
55 F. Safari-Alamuti, J. R. Jennings, M. A. Hossain, L. Y. L. Yung and Q. Wang, *Phys. Chem. Chem. Phys.*, 2013, **15**, 4767–4774.
56 A. Renaud, B. Chavillon, L. Cario, L. L. Pleux, N. Szuwarski, Y. Pellegrin, E. Blart, E. Gautron, F. Odobel and S. Jobic, *J. Phys. Chem. C*, 2013, **117**, 22478–22483.